CMTC-#486524-MS

# Numerical Analyses of the Effect of the Impurity in the Gas on the Solubility Trapping in the $CO_2$ Sequestration

Lingyu Mu, Xinwei Liao, Xiaoliang Zhao, Zhiming Chen, Langtao Zhu and Biao Luo, China University of Petroleum(Beijing), Beijing, China

Copyright 2017, Carbon Management Technology Conference

This paper was prepared for presentation at the Carbon Management Technology Conference held in Houston, Texas, USA, 17-20 July 2017.

This paper was selected for presentation by a CMTC program committee following review of information contained in an abstract submitted by the author(s). Contents of the paper have not been reviewed and are subject to correction by the author(s). The material does not necessarily reflect any position of the Carbon Management Technology Conference, its officers, or members. Electronic reproduction, distribution, or storage of any part of this paper without the written consent of the Carbon Management Technology Conference is prohibited. Permission to reproduce in print is restricted to an abstract of not more than 300 words; illustrations may not be copied. The abstract must contain conspicuous acknowledgment of CMTC copyright.

## Abstract

The $CO_2$ dissolved in the aquifer will increase the density of brine, which can result in the instability of the gravity and prompt the onset of the viscous finger. The viscous finger will lead to the convective mix, accelerating the process of $CO_2$ solution in the brine. However, the gas stream in the $CO_2$ storage usually contains the impurities such as $N_2$, $O_2$, and $SO_2$, which can change the density difference in the process of solution, and affect the solubility trapping in the $CO_2$ sequestration.

In this paper, a numerical simulation method was used to study the effect of different impurities on the solubility trapping in the process of $CO_2$ storage. Firstly, based on the PR-HV model, this paper calculated the solubility of $CO_2$, $N_2$, $O_2$, and $SO_2$ with different temperature and salinity and analysed the variation of the solubility. Then a multi-component numerical simulation model based on a certain aquifer layer was established to compare the $CO_2$ dissolution rate and the onset time of the instability and analyze the influence of impurities in the $CO_2$ stream on the solubility trapping. Finally, this paper clarified the impact on the $CO_2$ storage and suggested that the concentration of the impurities should be controlled in a rational range for the perspective of the economy and efficiency.

The results show that the solubility of $CO_2$ is higher than $N_2$ and $O_2$ in the saline water, and close to that of $SO_2$. We applied the solubility data to the numerical simulation. The results of the numerical simulation shows that with the increase of the concentration of $N_2$ or $O_2$, $CO_2$ dissolution rate has a decrease, and the onset time of the instability has an increase. It meas the longer time $CO_2$ plume keeping in the state of good flowing capability and low density. The onset of viscous finger will be postponed, leading to a negative influence on the solubility trapping and the risk of the $CO_2$ leak through fractures and faults. On the contrary, $SO_2$ can shorten the onset time of the instability, which accelerates the viscous finger and prompts the solubility trapping. A further conclusion is that the effect of $SO_2$ on the viscous fingering is more significantly than $N_2$ and $O_2$.

This paper deepens the understanding about the effect of the impure $CO_2$ on the solubility trapping, and clarifies the effect of different impurities.

# 1 Introduction

Global warming and greenhouse effect caused by the emission of $CO_2$ and other greenhouse gases are attracting more and more serious public concern. $CO_2$ capture and storage (CCS) is one of the most promising methods to reduce the emission of greenhouse gases, which refers to the process consisting of the separation of $CO_2$ from industrial and energy-related sources, transport to a storage location and long-term isolation from the atmosphere, shown in Figure 1. The CCS system consists of capture, transport, geological storage, ocean storage, mineral carbonation, industrial utilization, etc[1-6].

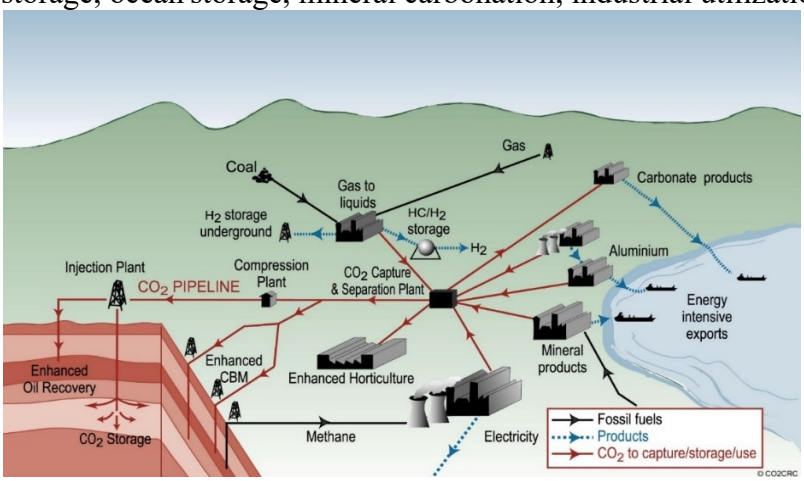


**Figure 1 Schematic diagram of CCS system**

Geological storage is generally regarded as the most mature and promising option for isolating the captured $CO_2$ from the atmosphere[7]. Geological storage means that $CO_2$ is stored in the geological structure, such as oil and gas fields, coal beds or deep saline water[7] ,as shown in Figure 2. $CO_2$ enhanced oil/gas (EOR/EGR) technology has been very mature with the development of the oil industry[9, 10]. Because of characteristics of the oil industry, $CO_2$ is generally used for recycling and a great quantity of gas will be produced to the ground with oil, which cannot meet the storage capacity requirements and long-term isolation. Coal beds stored with $CO_2$ need long-term isolation and cannot be mined for tens to hundreds of millions of years[3]. However, in hundreds of years, we may mine the coal beds due to advances in technology and energy demand, which means that $CO_2$ storage in coal beds has certain limitations. $CO_2$ stored in the deep saline water will not influence the ecosystem, and storage capacity is expected to reach 1000~10000 giga tons[11]. It is believed that deep saline formations have by far the largest capacity for $CO_2$ storage and are much more widespread than other options.

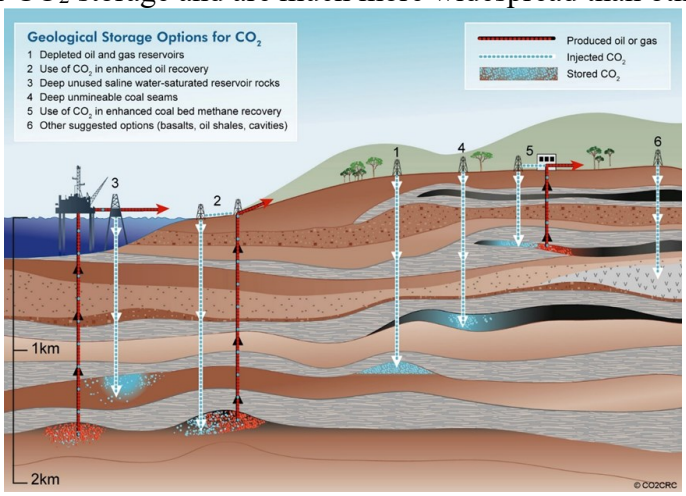


**Figure 2 Options for storing CO2 in deep underground geological formations**

There are four main mechanisms for geological storage of $CO_2$[3]. A low-permeability geological barrier such as mudstone or halite impedes the migration of buoyant $CO_2$ via high capillary pressure, which is

how the stratigraphic and structural trapping mechanism acts, shown in Figure 3 (a). However, $CO_2$ will enter the caprock when the pressure of the reservoir is high enough[3]. With the migration of $CO_2$, some $CO_2$ is trapped in the pores of rock due to the capillary pressure (gas-liquid interface tension)[12],shown in shown in Figure 3 (b). Residual trapping plays an important role at the early stage of $CO_2$ storage, for core-scale experiments show that residual trapping occurs in a few days or months[12]. When $CO_2$ dissolves into the saline water, the brine saturated with $CO_2$ is denser and will sink, shown in Figure 3 (c). The content of dissolved $CO_2$ will increase with time elapses. Solubility trapping is a major way for $CO_2$ geological storage, and the low flow rate of the formation water can ensure the stability of long-term storage[13]. $CO_2$ dissolved in the brine will react with rocks to form carbonate mineral precipitation, shown in Figure 3 (d), thus $CO_2$ is storaged with the most stable state[14, 15]. Although this chemical reaction exists at the early stage, mineral trapping is a rather long process that may last tens of thousands of years. The type of the trapping mechanism depends on the specific geological conditions, and in general it contains the mechanisms mentioned above. The occurrence of a specific mechanism depends on the length of time and migration of the $CO_2$.With the increase of time, the dominated trapping mechanism will change, and the security of $CO_2$ storage gradually increases, shown in Figure 4.

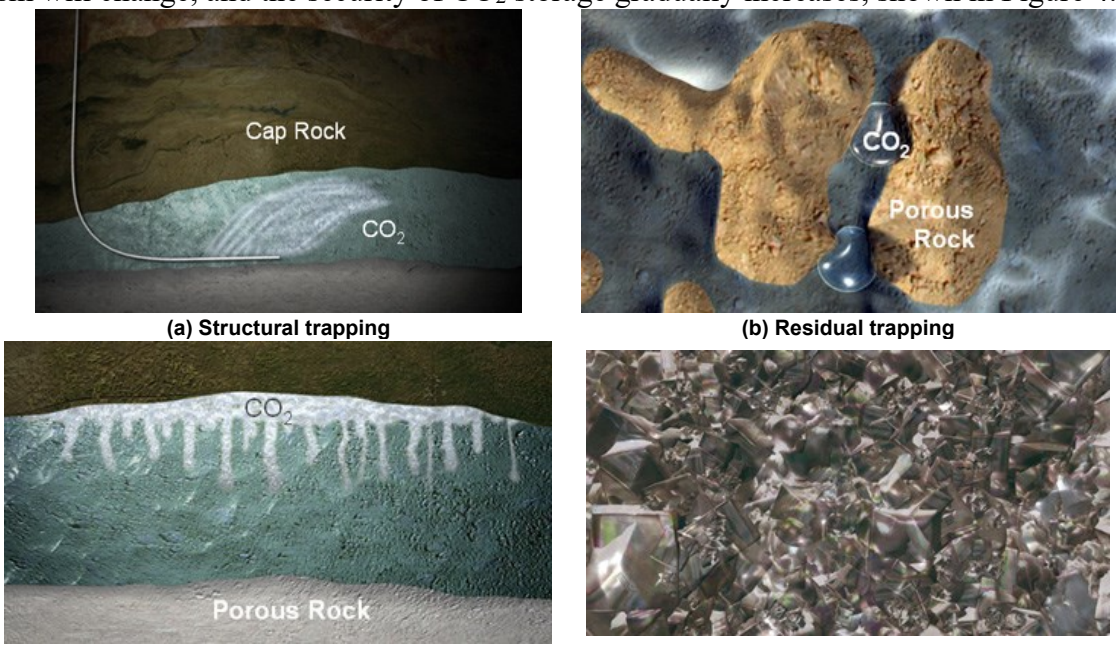


(a) Structural trapping (b) Residual trapping

(c) Solubility trapping (d) Mineral trapping

**Figure 3 Schematic diagram of mechanisms for geological storage of CO2**

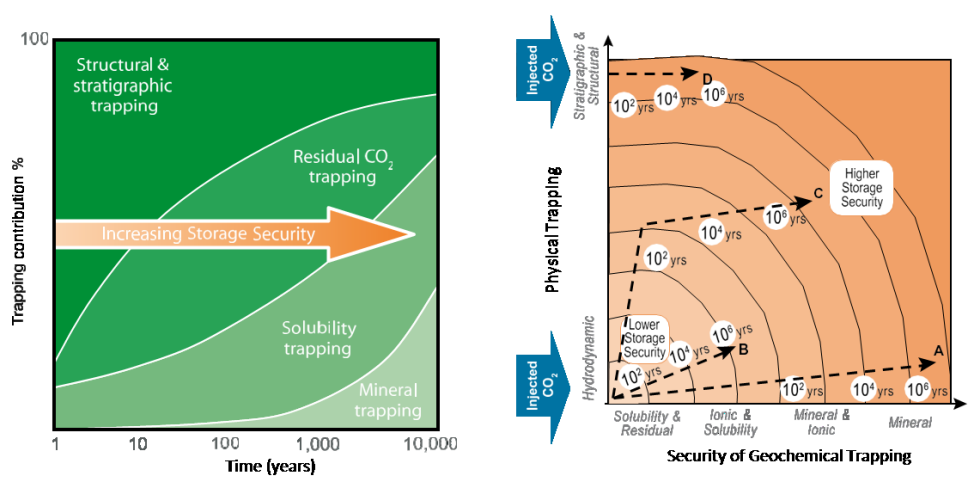


**Figure 4 Trapping contribution and security of physical and geochemical trapping mechanism**

For solubility trapping has a bearing on $CO_2$ geological storage, we mainly study the mechanism of the

solubility trapping in this paper. The dissolved $CO_2$ in the aquifer will increase the density of brine[16, 17]. The increase of the density is heterogeneous in the different part of the formation. A local increase of density, coupled with the heterogeneity of the aquifer such as permeability heterogeneity[18], will result in the instability of the gravity and prompt the onset of the viscous finger[19-22]. The viscous finger will lead to the convective mix, accelerating the process of $CO_2$ solution in the brine and reducing the possibility of $CO_2$ leakage. In view of its importance for long-term $CO_2$ storage, the convective mix driven by density difference has aroused many researchers' attention. Linear steady-state analysis and numerical simulation are two commonly used methods[23-27].

**Table 1 The range of contents of the impurities**

| Component | The range of contents, % | |
|---|---|---|
| | Capture after combustion | Capture before combustion |
| $CH_4$ | <0.010 | <0.035 |
| $N_2$ | <0.170 | <0.600 |
| $H_2S$ | trivial | <3.400 |
| CO | <0.001 | <0.400 |
| $O_2$ | <0.010 | trivial |
| $NO_x$ | <0.005 | / |
| $SO_x$ | <0.001 | / |
| $H_2$ | trivial | <3.000 |
| Ar | trivial | <0.050 |

Whichever method of is used to capture $CO_2$, the $CO_2$ stream contains a certain species and concentration of impurities, such as $N_2$, $O_2$, Ar, $SO_x$, $NO_x$, $H_2S$, $H_2$ and so on, which depends on the fuel used, the energy conversion process and the $CO_2$ capture technology[28]. The power industry is the main source of $CO_2$ emissions, whose main methods of $CO_2$ capture are capture after the combustion and capture before the combustion. The contents of the impurities[29] in the two methods are listed in Table 1. Even the smallest amount of the impurities could have a profound effect.

**Table 2 The properties of the gases**

| Component | Molar weight(g/mol) | Critical temperature(℃) | Critical pressure(MPa) |
|---|---|---|---|
| $CO_2$ | 44 | 31.04 | 7.38 |
| $SO_2$ | 64 | 157.49 | 7.88 |
| $O_2$ | 32 | -183.0 | 5.08 |
| $N_2$ | 28 | -147.05 | 3.39 |

The dissolution of $CO_2$ can increase the density of the formation fluid and cause convective mix[25, 26]. However, the physical and chemical properties of the impurities co-injected with $CO_2$ is markedly different with those of $CO_2$, which may have an impact on the process of $CO_2$ storage[30]. According to the content of the impurities, we choose $SO_2$, $O_2$ and $N_2$ as representative to study the effect of the impurities on the solubility trapping. The properties of $CO_2$, $SO_2$, $O_2$ and $N_2$ are listed in Table 2. The molar weight of the $SO_2$ is heavier than that of $CO_2$, while the molar weight of $O_2$ and $N_2$ are lighter. In other words, the increase of the density difference when $SO_2$ dissolves in the brine is bigger than that of the other three gases. The critical temperature and pressure of $O_2$ are lower than that of $CO_2$. Therefore, the mixture of $CO_2$ and $O_2$ will exist as supercritical fluid in the aquifer. Moreover, $N_2$ is in the same condition. $SO_2$ has a similar critical pressure with $CO_2$, while the critical temperature of $SO_2$ is rather

higher. However, the mixture of $CO_2$ and $SO_2$ can be regard as supercritical fluid considering the content of $SO_2$ in the mixture.

# 2 The dissolution law of the impurities

## 2.1 Theoretical model of solubility

Peng-Robinson equation of state cannot apply to the activity calculation of nonpolar substances. Besides, the application of Vander Waals mixing rule is limited, for the gas-liquid mixture is a non-ideal and highly asymmetric system[31]. Therefore, fugacity coefficient model established by Huron[32] and Peng-Robinson equation of state are adopted to characterize the thermodynamic properties of the CO2-water system. PR-HV model[33] is as followed:

$$p = \frac{RT}{v - b_m} - \frac{a_m}{v\left(v + b_m\right) + b_m\left(v - b_m\right)} \tag{1}$$

$$a_m = b_m\left[\sum_{i=1}^{n} x_i \frac{a_i \alpha_i}{b_i} - \frac{G_\infty^E}{c_0}\right] \tag{2}$$

$$b_m = \sum_{i=1}^{n} x_i b_i \tag{3}$$

$a_i$, $b_i$ and $\alpha_i$ are expressed by the following formulas:

$$a_i = 0.477235 \frac{R^2 T_{ci}^2}{p_{ci}} \alpha_i \tag{4}$$

$$b_i = 0.077796 \frac{RT_{ci}}{p_{ci}} \tag{5}$$

$$\alpha_i = \left[1 + m\left(1 - T_{ri}^{0.5}\right)\right]^2 \tag{6}$$

Without the defined pressure, the Gibbs free energy is calculated as follows:

$$G_\infty^E = \sum_{i=1}^{n} x_i \frac{\sum_{j=1}^{n} x_j C_{ji} G_{ji}}{\sum_{k=1}^{n} x_k G_{ki}} \tag{7}$$

According to the principle of chemical thermodynamics, the fugacity coefficient of component i with (T, p) as independent variable is:

$$RT \ln \varphi_i = \frac{\partial}{\partial n_i}\left[\int_{v_t}^{\infty}\left(p - \frac{nRT}{v_t}\right) dv_t\right] T, v_t, n_{j \neq i} - RT \ln Z \tag{8}$$

Then, the fugacity coefficient of the mixture calculated by PR-HV model is:

$$\ln \varphi_m = \frac{b_i}{b_m}\left(Z_m - 1\right) - \ln\left[Z_m\left(1 - \frac{b_m}{v_m}\right)\right] - \frac{1}{2\sqrt{2}RT}\left[\frac{a_i}{b_i} - \frac{RT \ln \gamma_i}{c_0}\right] \ln\left[\frac{v_m + \left(\sqrt{2} + 1\right) b_m}{v_m - \left(\sqrt{2} - 1\right) b_m}\right] \tag{9}$$

## 2.2 The dissolution of the gases in saline water

PR-VW model is used to calculate the solubility of $CO_2$, $SO_2$, $O_2$ and $N_2$ in different temperature and salinity. The solubility of $CO_2$, $SO_2$, $N_2$ and $O_2$ in pure water is listed in Table 3. The solubility of $N_2$ is

the smallest, and is the same order of magnitude as that of $O_2$. $SO_2$ is the most soluble within the impurities, whose solubility is about thousands of times than $N_2$ and scores of times than $CO_2$. With the temperature increases, the solubility of the gases decrease. The decreases in the solubility of $CO_2$, $SO_2$, $N_2$ and $O_2$ are 82.22%, 82.45%, 68.02%, and 67.09% respectively. The solubility of the gases in the saline water is shown in Figure 5, Figure 6, Figure 7 and Figure 8. With the salinity increases the solubility of the gases decrease.

**Table 3 The solubility of the gases in pure water**

| Temperature(℃) | solubility(g/kg) | | | |
|---|---|---|---|---|
| | $CO_2$ | $SO_2$ | $N_2$ | $O_2$ |
| 0 | 3.3333 | 228 | 0.0295 | 0.0691 |
| 10 | 2.5185 | 171 | 0.0243 | 0.0561 |
| 20 | 1.6889 | 114 | 0.0190 | 0.0435 |
| 30 | 1.2444 | 79 | 0.0160 | 0.0359 |
| 40 | 0.9778 | 56 | 0.0136 | 0.0309 |
| 50 | 0.7704 | 45 | 0.0112 | 0.0268 |
| 60 | 0.5926 | 40 | 0.0094 | 0.0227 |

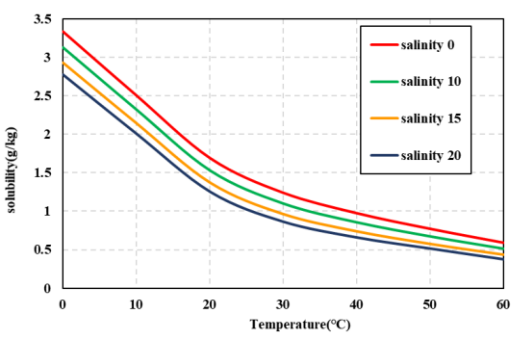


**Figure 5 The solubility of $CO_2$ in the saline water**

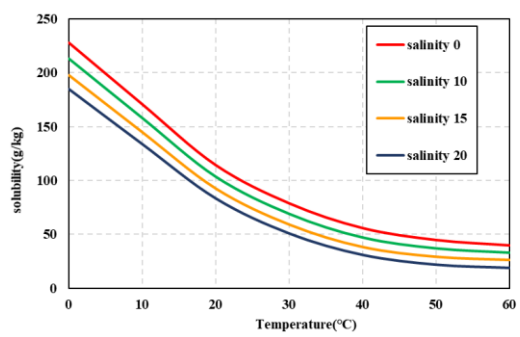


**Figure 6 The solubility of $SO_2$ in the saline water**

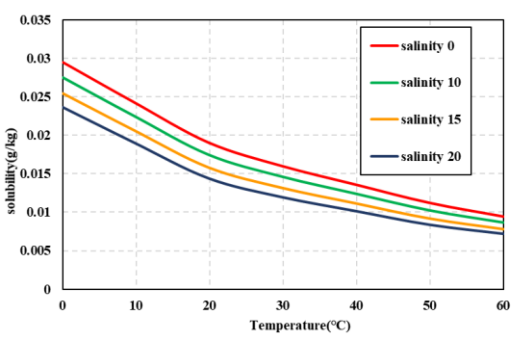


**Figure 7 The solubility of $N_2$ in the saline water**

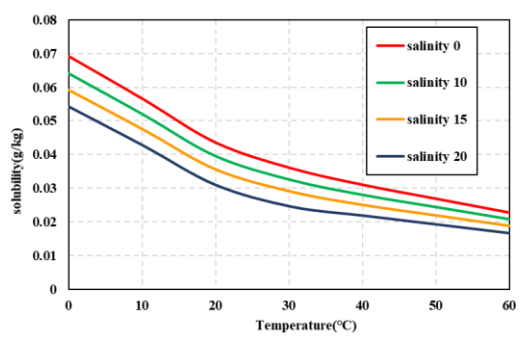


**Figure 8 The solubility of $O_2$ in the saline water**

## 2 Numerical simulation model

To study the effect of the impurities on the solubility trapping, a numerical simulation model is established to simulate the process of the solubility trapping in the $CO_2$ sequestration. The numerical model is established with the commercial software ECLIPSE 300. As shown in Figure 9, there is an impermeable caprock impeding the migration of buoyant $CO_2$ and the $CO_2$ stream is injected from the injection well to the saline water. The schematic diagram of the numerical simulation model is shown in Figure 10 and the parameters of the model is listed in Table 4.

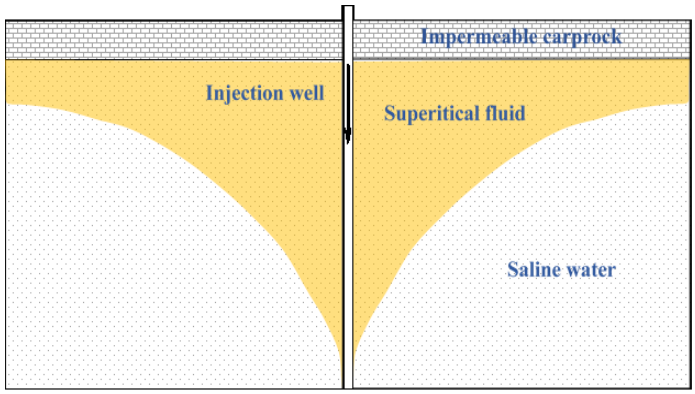


**Figure 9 Schematic diagram of the model**

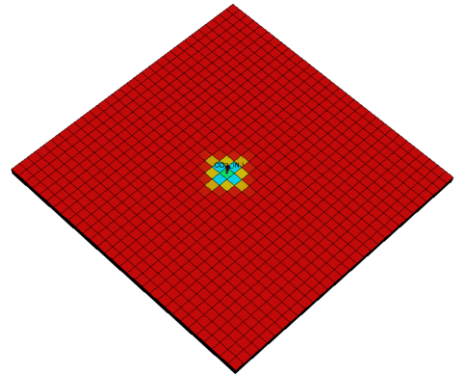

**Figure 10 Numerical simulation model**

**Table 4 Reservoir parameters**

| Reservoir parameters | Value | Reservoir parameters | Value |
|---|---|---|---|
| Size of the model | 30×10×30 | Rock compressibility | $5.8\times10^{-4}MPa^{-1}$ |
| Top depth | 1400m | Initial pressure | 17.4MPa |
| Porosity | 0.27 | Temperature | 32.2℃ |
| Permeability X | 400mD | irreducible water saturation | 0.3 |
| Permeability Y | 400mD | salinity | 0~20 |
| Permeability Z | 40mD | | |

Ten kinds of the compostions are set to study the impact of the concentration of the impurities, shown in Table 5. The range of the concentration of the impurities is 0% ~ 10% according to the composition of the $CO_2$ streams captured.

**Table 5 Injected gas compositions**

| Injected gas compositions | Dissolved gas compositions | | | |
|---|---|---|---|---|
| (mol%) | $CO_2$(×$10^{-5}$ mol%) | $SO_2$(×$10^{-5}$ mol%) | $N_2$(×$10^{-5}$ mol%) | $O_2$(×$10^{-5}$ mol%) |
| 100% $CO_2$ | 2095.30 | - | - | - |
| 98% $CO_2$+2%$SO_2$ | 2094.99 | 209.04 | - | - |
| 95% $CO_2$+5% $SO_2$ | 2094.19 | 516.12 | - | - |
| 90% $CO_2$+10% $SO_2$ | 2093.50 | 1020.48 | - | - |
| 98% $CO_2$+2% $N_2$ | 2047.20 | - | 4.52 | - |
| 95% $CO_2$+5% $N_2$ | 1981.70 | - | 8.79 | - |
| 90% $CO_2$+10% $N_2$ | 1876.80 | - | 14.62 | - |
| 98% $CO_2$+2% $O_2$ | 2049.48 | - | - | 7.31 |
| 95% $CO_2$+5% $O_2$ | 1983.98 | - | - | 11.58 |
| 90% $CO_2$+10% $O_2$ | 1879.08 | - | - | 17.41 |

## 3 Results and discussion

The change of the gas compositions is expected to have an impact on the convection process. Different compositions of the $CO_2$ streams will result in different density changes. According to the compositions of injection gases (Table 5), we can get the variations of density difference with different impurity concentrations, as shown in Figure 11.

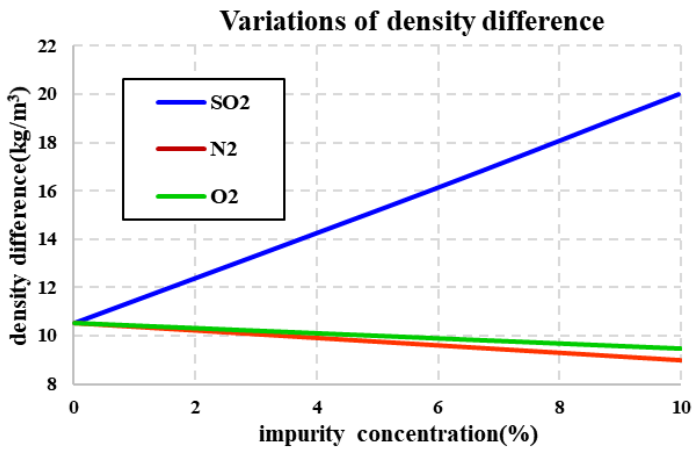


Figure 11 Variations of density difference

For the convective mix can accelerate the process of $CO_2$ solution in the brine and reduce the possibility of $CO_2$ leakage, Onset time of the instability represents the validity of the solubility trapping mechanism to a certain extent. There is no commonly accepted definition of onset time of the instability. According to the method proposed by George S.H. Pau[34], onset time of the instability is defined as the time when dissolution rate, referring to $CO_2$ molar flux from top boundary to the simulated region, is 2% higher than diffusive flux. Although the process of the convection is complicated and it is difficult to quantify, the total inventory of $CO_2$ dissolved into the saline water is rather stable and measured. Eventually, we choose dissolution rate, onset time and total inventory dissolved as the parameters of the impacts of different $SO_2$, $N_2$ and $O_2$ concentrations on solubility trapping.

### 3.1 Dissolution rate and onset time of the instability

The dissolution rate of $CO_2$ is an important parameter of solubility trapping. As shown in Figure 12, Figure 13 and Figure 14, the dissolution rate can be divided into three stages. These are diffusion-dominated stage, convection-dominated stage and convection-decay stage. Before the process of the convection, the downward transport of the dissolved gas is dominated by molecular diffusion and the dissolution rate decays at the rate of $t^{-0.5}$.

At this stage, the concentrations of the impurities have a limited influence on the dissolution rate. The dissolution rate decreases slightly with the increase of the concentrations of $N_2$ and $O_2$ (Figure 13 and Figure 14). At the convection-dominated stage, due to the collision, fusion and merging of the viscous finger, the dissolution rate curve exhibits a significant irregular change, which also denotes the inherent instability of the convection process. At this stage, the effect of the impurities on the dissolution rate is much greater than the diffusion-dominated stage. $N_2$ and $O_2$ will reduce the dissolution rate of $CO_2$ stream and $SO_2$ will increase the dissolution rate on the contrary. With the increase of concentration of the $SO_2$, the dissolution rate will increase. By contrast, the dissolution rate will decrease with the increase of the concentration of $N_2$/ $O_2$. Under the same impurity concentration, the variation of the dissolution rate of $CO_2$-$SO_2$ system is much larger than that of $CO_2$-$N_2$ system or $CO_2$-$O_2$ system. At the convection-decay stage, the dissolution rate decreases and molecular diffusion becomes the dominant fluid transport mechanism again. As a result, the difference among the dissolution rates of the impurities are also quite small.

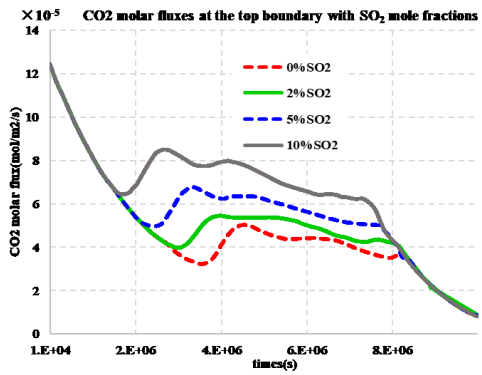


Figure 12 $CO_2$ molar fluxes with $SO_2$ mole fractions

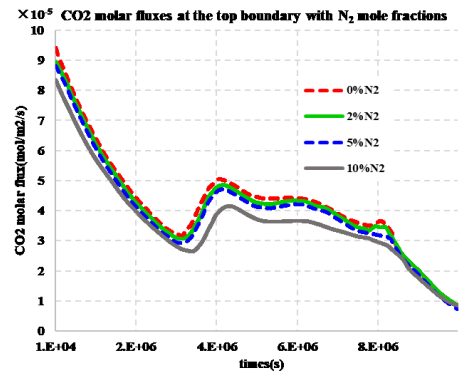


Figure 13 $CO_2$ molar fluxes with $N_2$ mole fractions

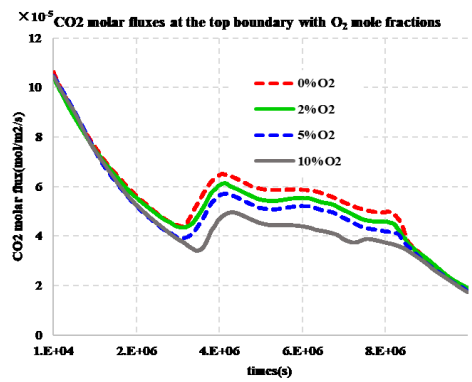


Figure 14 $CO_2$ molar fluxes with $O_2$ mole fractions

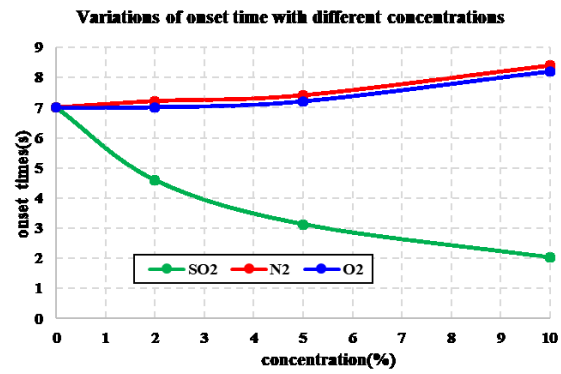


Figure 15 Onset time with different concentrations

Figure 15 shows the onset time of the impurities with different concentrations. With the increase of concentration of the impurities, the onset time of $CO_2$-$SO_2$ system decreases and the onset time of $CO_2$-$N_2$ / $CO_2$-$O_2$ system increases. Moreover, the decrease of onset time of $CO_2$-$SO_2$ system is greater than the increase of the $CO_2$-$N_2$ system and $CO_2$-$O_2$ system increases. The increase of onset time of $CO_2$-$N_2$ system is slightly greater than that of $CO_2$-$O_2$ system. The inclusion of $N_2$ and $O_2$ in the $CO_2$ streams delays the onset time, which is negative to the dissolution of $CO_2$ and the solubility trapping mechanism. $SO_2$ will encourage the convection and is conducive to $CO_2$ storage.

### 3.2 Total inventory of $CO_2$ dissolved

The total inventory of $CO_2$ dissolved into the saline water is stable and can be used to measure the efficiency of solubility trapping mechanism. Figure 16, Figure 17 and Figure 18 show the $CO_2$ inventory with different concentrations of the impurities at the early stage. Figure 19, Figure 20 and Figure 21 show the $CO_2$ inventory with different concentrations of the impurities at the end of the simulations. Since the convection can increase the dissolution rate of $CO_2$ largely, the total inventory of $CO_2$ dissolved is much larger than the total inventory of $CO_2$ diffused after the onset of the convection. At the diffusion-dominated stage, the total inventory of $CO_2$ dissolved is equivalent to the total inventory of $CO_2$ diffused. With the concentration of $SO_2$ increasing, the total inventory of $CO_2$ increases significantly. With the concentration of $N_2$ and $O_2$ increasing, the total dissolved CO2 inventory decreases slightly.

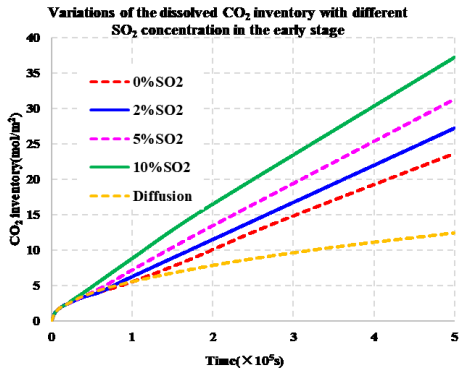


Figure 16 $CO_2$ molar fluxes with $SO_2$ mole fractions

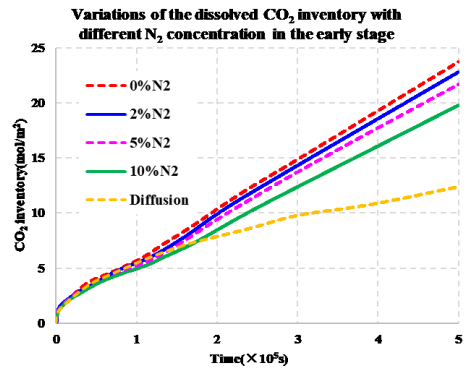


Figure 17 $CO_2$ molar fluxes with $N_2$ mole fractions

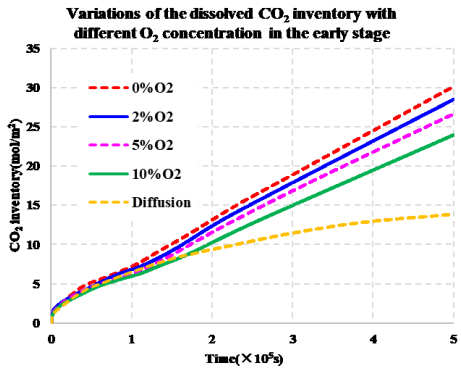


Figure 18 $CO_2$ molar fluxes with $O_2$ mole fractions

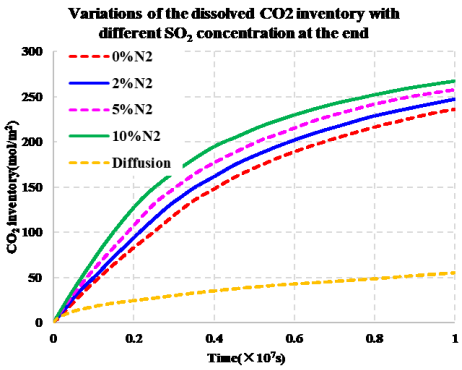


Figure 19 $CO_2$ molar fluxes with $SO_2$ mole fractions

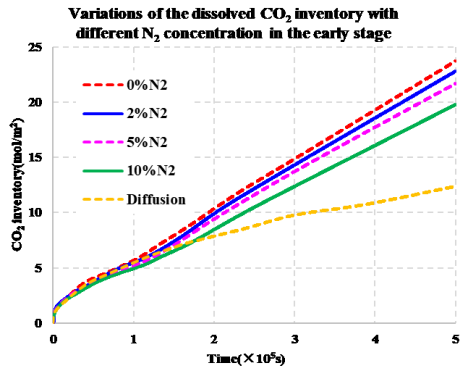


Figure 20 $CO_2$ molar fluxes with $N_2$ mole fractions

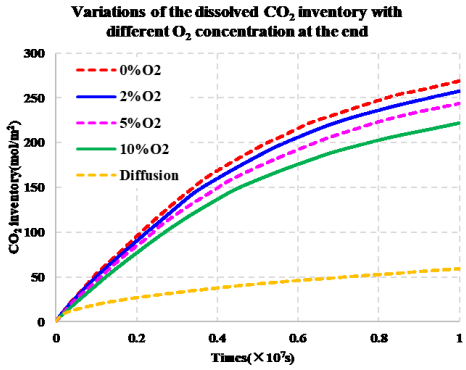


Figure 21 $CO_2$ molar fluxes with $O_2$ mole fractions

## 3.3 The effect of the salinity

According to the dissolution rule of the impurities in the brine mentioned above, with the salinity increases the solubility of the gases decrease, which will decrease the dissolution rate of the $CO_2$. The

increase of the salinity will lead to the decrease of onset time of the instability, shown in Figure 22. Furthermore, total inventory of $CO_2$ dissolved will decrease with the increase of the salinity, shown in Figure 23.

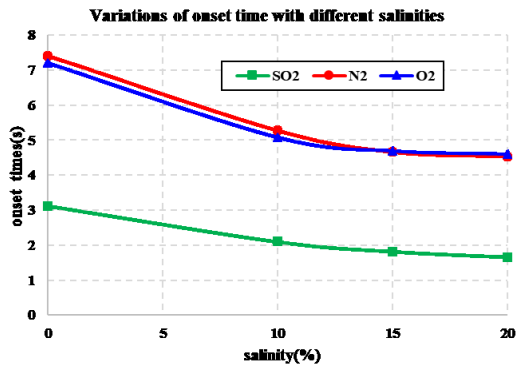


Figure 22 $CO_2$ molar fluxes with $SO_2$ mole fractions

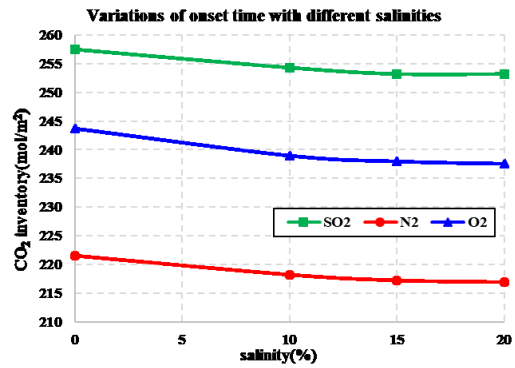


Figure 23 $CO_2$ molar fluxes with $N_2$ mole fractions

## 4 Conclusions and future work

The presence of impurities in the $CO_2$ have a significant impact on the $CO_2$ storage. It will be costly to remove the impurities in the $CO_2$ stream. So allowing the presence of impurities in the $CO_2$ streams will cut down the cost of the $CO_2$ capture. However, the impurities have a complex effect on the process of the $CO_2$ storage. In this paper, a numerical simulation model considering dissolution and diffusion is established by Eclipse to simulate the effect of the impurities on the solubility trapping. The convection driven by the density difference will encourage the dissolution of $CO_2$ and increase the dissolution rate apparently in the solubility trapping mechanism. The dissolution of gas in the aquifer will change the density of brine. $SO_2$ is the most soluble within the impurities, whose solubility is about thousands of times than $N_2$ and scores of times than $CO_2$.moreover, the salinity of the formation water have a significant effect on the solubility. The density difference caused by the gases will have a variation. When the gases is co-injected with $CO_2$ into the formation, the process of solubility trapping will be influenced.With the concentration of $O_2$ or $N_2$ increasing, the onset time of the instability will be postponed. The dissolution rate and the total inventory of $CO_2$ dissolved into the formation water will decrease. On the contrary, $SO_2$ will reduce the onset of the instability and increase the dissolution rate and the total inventory. In a word, $SO_2$ is conducive to $CO_2$ storage, while $N_2$ and $O_2$ are negative to the $CO_2$ storage. Besides, the effect of $SO_2$ is more obvious than that of $O_2$ and $N_2$ under the same circumstance. The concentration of the impurities should be controlled in a rational range for the perspective of the economy and efficiency.

## Nomenclature

***p*** *pressure(MPa)*
***T*** *temperature(℃)*
***R*** *general gas constant(8.3147MPa·cm$^3$/(mol·K))*
$a_m$ *gravitational constant of the mixed systems*
$b_m$ *repulsive constants of the mixed system*
***v*** *molar volume(cm$^3$/mol)*
***n*** *mole of the system*
$x_i$ *mole fraction of i component in the liquid*
$a_i$ ,$b_i$ *parameters of EOS of i component*
$\alpha_i$ *a function about temperature*
$G_\infty^E$ *excess Gibbs Free Energy under Infinite Pressure(J/mol)*

$c_0$ *constant*$\left(=\frac{1}{2\sqrt{2}_m}\ln\frac{2+\sqrt{2}}{2-\sqrt{2}}\right)$

$T_{ci}$ *critical temperature of the i component(℃)*

$p_{ci}$ *critical pressure of the i component(MPa)*

$T_{ri}$ *reduced temperature of the i component(℃)*

$p_{ri}$ *reduced pressure of the i component(MPa)*

$m$ *a function about acentric factor*

$C_{ji}$ $C_{ji}= g_{ji} - g_{ii}$

$g_{ji}, g_{ii}$ *Boltzmann factor between molecules*

$k_{ij}$ *interaction coefficient between i component and j component*

$G_{ji}, G_{ki}$ *temperature-dependent parameters that can be adjusted*

$\alpha_{ji}, \alpha_{ki}$ *non-random parameters between i, j components and between i, k components*

$\varphi_i$ *fugacity coefficient of i component*

$Z$ *deviation factor*

$n_i, n_j$ *mole fraction of i, j component*

$\varphi_m$ *fugacity coefficient of the mixture*

$Z_m$ *deviation factor of the mixture*

$\gamma_i$ *activity coefficient of i component*

## Acknowledgement

This work is supported by Science Foundation of China University of Petroleum, National Basic Research 973 Program of China (2015CB250900), and National Natural Science Foundation of China (U1262101).

## Reference

[1] Holloway S. Carbon dioxide capture and geological storage[J]. Philosophical Transactions of the Royal Society A: Mathematical, Physical and Engineering Sciences. 2007, 365(1853): 1095-1107.

[2] De Silva P N K, Ranjith P G. A study of methodologies for CO2 storage capacity estimation of saline aquifers[J]. Fuel. 2012, 93: 13-27.

[3] Metz B, Davidson O, De Coninck H, et al. IPCC special report on carbon dioxide capture and storage[Z]. Intergovernmental Panel on Climate Change, Geneva (Switzerland). Working Group III, 2005.

[4] Burnside N M, Naylor M. Review and implications of relative permeability of CO2/brine systems and residual trapping of CO2[J]. International Journal of Greenhouse Gas Control. 2014, 23: 1-11.

[5] Bachu S. CO2 storage in geological media: Role, means, status and barriers to deployment[J]. PROGRESS IN ENERGY AND COMBUSTION SCIENCE. 2008, 34(2): 254-273.

[6] Leung D, Caramanna G, Maroto-Valer M M. An overview of current status of carbon dioxide capture and storage technologies[J]. RENEWABLE & SUSTAINABLE ENERGY REVIEWS. 2014, 39: 426-443.

[7] Michael K, Golab A, Shulakova V, et al. Geological storage of CO2 in saline aquifers-A review of the experience from existing storage operations[J]. INTERNATIONAL JOURNAL OF GREENHOUSE GAS CONTROL. 2010, 4(4): 659-667.

[8] Bachu S, Adams J J. Sequestration of CO2 in geological media in response to climate change: capacity of deep saline aquifers to sequester CO2 in solution[J]. 2003, 44(20): 3151-3175.

[9] Shen P P, Liao X W. The Technology of Carbon Dioxide Stored in Geological Media and Enhanced Oil Recovery[J]. 2009.

[10] Bachu S, Shaw J C, Pearson R M. Estimation of Oil Recovery and CO2 Storage Capacity in CO2 EOR Incorporating the Effect of Underlying Aquifers[J]. Society of Petroleum Engineers Journal. 2004.

[11] Birkholzer J T, Zhou Q L, Tsang C F. Large-scale impact of CO2 storage in deep saline aquifers: A sensitivity study on pressure response in stratified systems[J]. INTERNATIONAL JOURNAL OF GREENHOUSE GAS CONTROL. 2009, 3(2): 181-194.

[12] Ghesmat K, Hassanzadeh H, Abedi J. The effect of anisotropic dispersion on the convective mixing in long - term CO2 storage in saline aquifers[J]. 2011, 57(3): 561-570.

[13] Spycher N, Pruess K, Ennis-King J. CO2-H2O mixtures in the geological sequestration of CO2. I. Assessment and calculation of mutual solubilities from 12 to 100°C and up to 600 bar[J]. 2003, 67(16): 3015-3031.

[14] Bachu S, Gunter W D, Perkins E H. Aquifer disposal of CO 2: hydrodynamic and mineral trapping[J]. Energy Conversion and Management. 1994, 35(4): 269-279.
[15] Oelkers E H, Gislason S R, Matter J. Mineral Carbonation of CO2[J]. ELEMENTS. 2008, 4(5): 333-337.
[16] Bachu. CO2 storage in geological media: role, means, status and barriers to deployment [J]. Progress in Energy and Combustion Science. 2008, 2(34): 254-273.
[17] Gilfillan S, Lollar B S, Holland G, et al. Solubility trapping in formation water as dominant CO2 sink in natural gas fields[J]. NATURE. 2009, 458(7238): 614-618.
[18] Lengler U, De Lucia M, K Hn M. The impact of heterogeneity on the distribution of CO2: Numerical simulation of CO2 storage at Ketzin[J]. International Journal of Greenhouse Gas Control. 2010, 4(6): 1016-1025.
[19] Elenius. Convective mixing in geological carbon storage[Z]. 2011.
[20] Sainz-Garcia A, Abarca E, Nardi A, et al. Convective mixing fingers and chemistry interaction in carbon storage[J]. International Journal of Greenhouse Gas Control. 2017, 58: 52-61.
[21] Torabi M, Peterson G P, Torabi M, et al. A thermodynamic analysis of forced convection through porous media using pore scale modeling[J]. International Journal of Heat and Mass Transfer. 2016, 99: 303-316.
[22] Emami-Meybodi H. Stability analysis of dissolution-driven convection in porous media[J]. Physics of Fluids. 2017, 29(1): 14102.
[23] Jiang X. A review of physical modelling and numerical simulation of long-term geological storage of CO2[J]. Applied Energy. 2011, 88(11): 3557-3566.
[24] Ennis-King J P, Paterson L. Role of Convective Mixing in the Long-Term Storage of Carbon Dioxide in Deep Saline Formations[J]. Spe Journal. 2005, 10(3): 349-356.
[25] Ennis-King J, Paterson L. Coupling of geochemical reactions and convective mixing in the long-term geological storage of carbon dioxide[J]. International Journal of Greenhouse Gas Control. 2007, 1(1): 86-93.
[26] Ennisking J, Preston I, Paterson L. Onset of convection in anisotropic porous media subject to a rapid change in boundary conditions[J]. Physics of Fluids. 2005, 17(8): 239-248.
[27] Meng Q, Jiang X. Numerical analyses of the solubility trapping of CO2 storage in geological formations[J]. Applied Energy. 2014, 130: 581-591.
[28] White C M, Strazisar B R, Granite E J, et al. Separation and capture of CO2 from large stationary sources and sequestration in geological formations - Coalbeds and deep saline aquifers[J]. JOURNAL OF THE AIR & WASTE MANAGEMENT ASSOCIATION. 2003, 53(6): 645-715.
[29] Oosterkamp. State-of-the-Art Overview of CO2 Pipeline Transport with relevance to offshore pipelines[Z]. Norway: PolytecR & DFoundation, 2008.
[30] Li D, Jiang X. A numerical study of the impurity effects of nitrogen and sulfur dioxide on the solubility trapping of carbon dioxide geological storage[J]. Applied Energy. 2014, 128: 60-74.
[31] Yan W, Huang S, Stenby E H. Measurement and modeling of CO2 solubility in NaCl brine and CO2 – saturated NaCl brine density[J]. International Journal of Greenhouse Gas Control. 2011, 5(6): 1460-1477.
[32] Marie-José H. New mixing rules in simple equations of state for representing vapour-liquid equilibria of strongly non-ideal mixtures[J]. Fluid Phase Equilibria. 1979.
[33] Dali H. Experimental research and theoretical model for CO2 solubility in water under high temperature and high pressure[J]. 2015.
[34] Pau G S H, Bell J B, Pruess K, et al. High-resolution simulation and characterization of density-driven flow in CO2 storage in saline aquifers[J]. Advances in Water Resources. 2010, 33(4): 443-455.